Predictions of the Geometries and Fluorescence Emission Energies of Oxyluciferins

Tianxiao Yang and John D. Goddard*

Department of Chemistry, University of Guelph, Guelph, Ontario, Canada, N1G 2W1

Received: December 12, 2006; In Final Form: March 1, 2007

The complete active space self-consistent field (CASSCF) method and multiconfigurational second-order perturbation theory (CASPT2) have been used to study the structures and spectra of oxyluciferins ($OxyLH_2$). The ground and lowest-lying singlet excited states geometries have been optimized using CASSCF. CASPT2 has been used to predict relaxed emission energies. The focus is on the lowest-lying singlet excited states of the anionic keto and enol forms of $OxyLH_2(-1)$ at the optimized excited-state geometries. The planar keto and enol forms of $OxyLH_2(-1)$ are minima on both the S_0 and the S_1 potential energy surfaces. The twisted keto and enol forms of $OxyLH_2(-1)$ are transition states on the S_0 and S_1 potential energy surfaces. The $S_1 \rightarrow S_0$ fluorescence emission energies are in the range of 54.2−58.4 kcal/mol for the anionic planar keto forms of $OxyLH_2$, and in the range of 55.7−63.2 kcal/mol for the anionic enol forms of $OxyLH_2$. S_0 and S_1 potential energy surfaces and thus are not implicated in the emission spectra in the gas phase.

1. Introduction

In nature, bioluminescence emission by firefly luciferases can produce different colors, ranging from red to yellow to green. It has been suggested that the major factor that determines the bioluminescence color is the microenvironment of the emitter in the enzyme active site. Elucidation of the relationship between the structure of the light emitter and the fluorescence spectra is of both theoretical and practical interest. The change in bioluminescence color caused by subtle structural differences in the luciferases has attracted much research interest.[1−15] However, the detailed mechanism of the changes in the bioluminescence color is still unclear.

White et al.[2,7] proposed that red light may be ascribed to the keto form of excited-state oxyluciferin and green light to the corresponding enol form. The resultant color depends on the keto−enol equilibrium. However, Branchini et al.[3,8] presented evidence that a single emitter in the keto form could account for the range of bioluminescence color observed in nature. These experimental findings could be explained by the proposal of McCapra et al.[4] that color modulation is associated with conformations of the keto form of oxyluciferin created by rotation about the central C2−C2′ bond. Red emission is attributed to the minimum energy conformation of an unusual twisted intramolecular charge-transfer excited state in which the rings of oxyluciferin are perpendicular to each other. Yellow-green light emission would result from a higher energy excited-state conformer with coplanar rings. Luciferase-emitter interactions could maintain specific conformations in the excited state, thereby influencing the emission color. According to their results,[3,4,8] the keto form in the excited singlet state has a twisted structure rather than a planar one. Extensive experimental findings show that the color of the light emission from $OxyLH_2$ depends on the pH of the media.[8−10] The fluorescence spectra of luciferin and its analogs are affected by the nature of the solvent.[6,12−14] The fluorescence spectrum in solvents of distinct dielectric constants can be shifted as much as 40 nm, suggesting that similar differences in the luciferase active-site microenvironment can affect the bioluminescence.[6] Very recently, Nakatsu et al.[15] reported several X-ray crystal structures of a luciferase from Japanese Genje-botaru firefly. The structural data support a model that explains how small changes in the protein change the color of the emitted light. Their findings indicate the degree of rigidity of the excited-state of oxyluciferin determines the color of bioluminescence during the chemical reaction preceding the emission. There are at least two different excited states, one of higher energy emitting yellow-green light and the other of lower energy emitting red light.

Oxyluciferin is extremely unstable, and thus it is very difficult to study experimentally the light emitters and especially to determine their geometries. Quantum chemical methods are important in understanding both the spectroscopy and structures of the light emitters. To our knowledge, theoretical studies of bioluminescent phenomena are limited[4a,16] due largely to practical difficulties in carrying out geometry optimizations for excited states.

Reliable predictions of excited-state properties require the optimization of the excited-state geometries, as discussed, for example, by Parusel et al.[17] and Rappoport et al.[18] Modern computational chemistry offers a number of methods for describing electronically excited states. However, the accurate prediction of excited electronic states has been a challenge. Relatively few quantum chemical methods are available for geometry optimizations of the excited states of larger polyatomic molecules. Configuration interaction with single excitations (CIS)[19] allows the optimization of the excited-state geometries of relatively large molecules. However, predicted excited-state properties often are not in quantitative agreement with experiment.[17] Our previous theoretical predictions of excitation and fluorescence energies with CIS on oxyluciferins needed to be corrected empirically to agree with experiment.[20,21]

In our previous work,[20,21] the Hartree−Fock (HF) method was employed to optimize the ground state geometries and the CIS method for the excited-state geometries. Time dependent density functional theory (TDDFT)[22,23] was used to calculate the absorption and emission spectra of the anionic and neutral

* Corresponding author. Tel: +1 519 824 4120, ext. 53102. Fax: +1 519 766 1499. E-mail: jgoddard@uoguelph.ca.

10.1021/jp068542b CCC: $37.00
Published on Web 04/24/2007

planar keto and enol forms of $OxyLH_2$. Predicted properties included the geometries, the vertical excitation energies, and the vertical electronic absorption and emission spectra. Solvation effects on the electronic absorption and emission spectra of luciferin and oxyluciferin also were discussed.[21] The DFT and TDDFT methods achieved good accuracies for the geometries of the ground states and for the electronic absorption spectra. However, the TDDFT method did not predict well the excited states of the twisted keto and enol form of $OxyLH_2(-1)$. The TDDFT/CIS method predicted that in the S_1 state, the twisted keto form of $OxyLH_2(-1)$ was 27.1 and 20.3 kcal/mol lower in energy than the keto-s-*cis*(-1) and keto-s-*trans*(-1) forms. The vertical emission energy of keto-s-*twist*(-1) form was predicted to be only 14.5 kcal/mol,[24] which is far too small relative to experiment.

A closed-shell singlet state can be described by a single-determinant. An open-shell singlet, however, formally cannot be expressed as a single-determinant (such as in conventional Kohn−Sham DFT) and requires at least two determinants. Such states are not well-described by TDDFT within the adiabatic approximation and with the usual exchange-correlation functionals.[25] Furthermore, charge-transfer valence-excited states might occur with the oxyluciferin molecules.[16] It is known that TDDFT tends to underestimate considerably these charge-transfer excitation energies[26,27] due to spurious self-interaction.[28] Tozer et al.[25] found that TDDFT method did not predict accurately some valence excited states of unsaturated organic compounds involving such charge transfer.

TDDFT and CIS methods are generally not considered accurate enough for definitive conclusions on charge transfer, which could be important in bioluminescence. The complete-active-space self-consistent-field (CASSCF)[29] method in which the wave function is obtained as a full configuration interaction (CI) expansion in an active orbital space is a potentially reliable method for geometry optimization of electronic excited states. It offers great flexibility in describing electronic structures. The CASSCF method is able to adequately account for important nondynamic electron correlation effects caused by nearly degenerate configurations. The contribution of additional dynamic correlation is computed by multiconfigurational complete active space second-order perturbation theory (CASPT2).[30,31] The CASSCF method can be used to predict accurate electronic structures for both ground and excited states and is well suited to describe photochemical reactions. We use the CASSCF method to optimize the geometries of the ground and the lowest-lying singlet-excited electronic states of two possible light emitters, the anionic keto form and enol forms of $OxyLH_2$-(-1). With the CASSCF multireference wavefunctions, CASPT2 is used to include dynamic electron correlation corrections, which are often important for obtaining quantitatively accurate results, for excitation and fluorescence energies.

2. Computational Details

For consistency with previous calculations as well as practical computational limitations, the 6-31G(d) basis sets were used for all atoms.[32,33] Inclusion of diffuse functions often is recommended for the accurate prediction of excitation energies. However, because the molecules we are investigating have no symmetry, i.e., are of C_1 symmetry, computations with larger basis sets containing diffuse functions were not possible due to limitations in the CASSCF software. The neglect of diffuse functions should be possible since all computations would show similar influences from these functions.

The CASSCF method was used in geometry optimizations on the ground and the lowest-lying singlet excited states. For the singlet excited-state geometry optimization, the CASSCF wave functions were obtained by a state-averaged CASSCF calculation, including the lowest singlet excited-state and the ground state with equal weights. CASSCF computations were done with different CAS spaces: six active electrons in six orbitals (three HOMO and three LUMO orbitals), eight active electrons in eight orbitals (four HOMO and four LUMO orbitals), and ten active electrons in ten orbitals (five HOMO and five LUMO orbitals). Dynamic electron correlation can be important for excitation energies. At the CASSCF optimized geometries the multistate CASPT2 (MS-CASPT2) method, based on reference wave functions obtained by state-averaged CASSCF calculations, was adopted. MS-CASPT2 uses the same state-averaging and active spaces as in the CASSCF calculations.

CASSCF geometry optimizations were run without symmetry constraints, and all orbitals are optimized. Default convergence criteria implemented in the respective programs were used throughout.

The vibrational frequency analysis for the ground state was conducted with the MCKINLEY and MCLR programs.[34] Oscillator strengths within the CAS approach were obtained with the RAS state interaction program (RASSI).[35,36] All predictions were made with the MOLCAS 6.4 program package.[37]

3. Results and Discussion

3.1. Ground and Lowest-Lying Singlet Excited State Geometries of the Anionic Keto Forms of Oxyluciferin. The ground states of three possible anionic keto forms of $OxyLH_2$, keto-s-*trans*(-1), keto-s-*cis*(-1), and keto-s-*twist*(-1), were optimized using the CASSCF method with different active spaces, CASSCF(6,6), CASSCF(8,8), and CASSCF(10,10). The geometrical parameters computed with these different CAS spaces are presented in Figure 1 and collected in Table 1. These results indicate that both keto-s-*trans*(-1) and keto-s-*cis*(-1) have nearly planar ring structures in their ground states with all the sizes of CASSCF. Vibrational frequency analysis illustrates that the rigorously planar structures for both the keto-s-*trans*(-1) and the keto-s-*cis*(-1) ground states are minima since all vibrational frequencies are real. The keto-s-*twist*(-1) structure is predicted to be a transition state with one imaginary frequency. CASSCF(6,6), CASSCF(8,8), and CASSCF(10,10) predict the C2−C2′ bond distances between the benzothiazolyl and the thiazole fragments to be 1.371, 1.377 and 1.385 Å for keto-s-*cis*(-1), and 1.367, 1.369, and 1.371 Å for keto-s-*trans*-(-1). Larger CAS spaces predict slightly longer C2−C2′ bond distances. The other geometrical parameters are almost identical with the different CASSCF spaces. For keto-s-*twist*(-1), it is the benzothiazolyl and thiazole rings which are twisted relative to each other. The C2−C2′ bond distance is 1.480 Å with CASSCF(6,6) and 1.482 Å with CASSCF(8,8) or CASSCF-(10,10). The NCCN and SCCS torsion angles are 85.13° and 82.16°, 86.20° and 82.55°, and 86.07° and 82.59° with CASSCF(6,6), CASSCF(8,8), and CASSCF(10,10). It is notable that the C2−C2′ bond distances predicted by the CASSCF method are shorter than those from by the CIS and B3LYP methods.[20,21] The C2−C2′ distances in keto-s-*trans*(-1) and keto-s-*cis*(-1) were 1.409 and 1.417 Å with CIS/6-31G* method, and 1.412 and 1.419 Å with B3LYP/6-31+G* method.[20,21]

State-averaged CASSCF calculations, which weigh equally the ground and the lowest-lying singlet excited states, were used for geometry optimization of the first singlet excited state. The optimized equilibrium geometries of the first singlet excited-

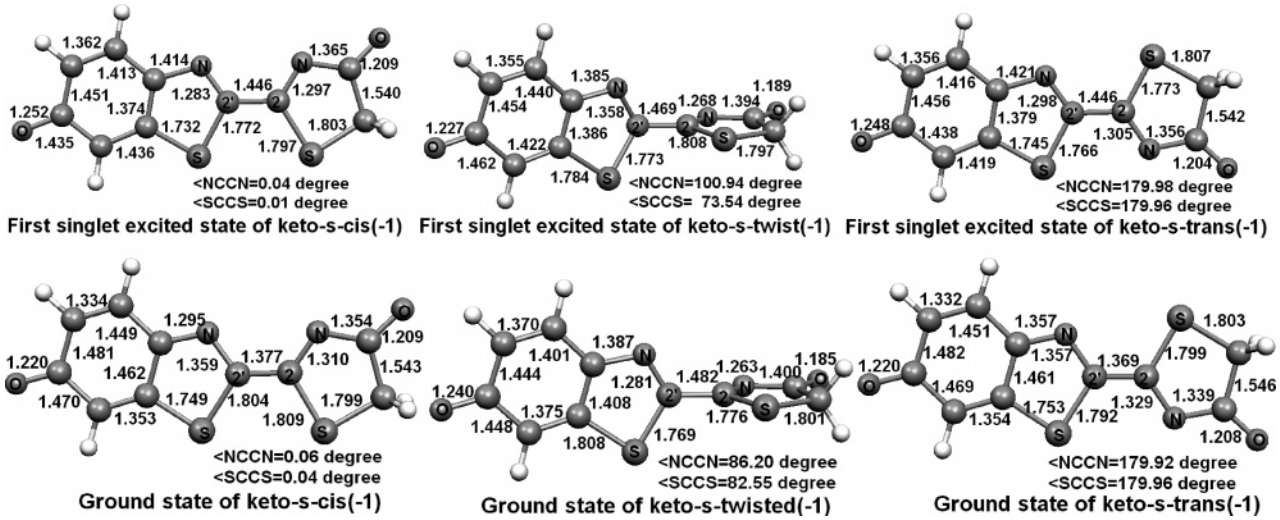

Figure 1. Geometries optimized at the CASSCF(8,8) level for the ground and lowest-lying singlet excited states of anionic keto forms of oxyluciferins.

TABLE 1: Key Geometrical Parameters of the Keto Forms of $OxyLH_2(-1)$ for the Ground (S_0) and Lowest-Lying Singlet Excited (S_1) States Predicted by Different Levels of CASSCF

theoretical level	state	C2−C2′ (Å)	C2′−N (Å)	C2−N (Å)	C2′−S (Å)	C2−S (Å)	C═O (Å)	NCCN (deg)	SCCS (deg)
				Keto-s-*cis*(−1)					
CASSCF(6,6)	S_1	1.448	1.281	1.299	1.772	1.792	1.225	0.16	0.15
	S_0	1.371	1.363	1.317	1.802	1.805	1.208	0.02	0.02
CASSCF(8,8)	S_1	1.446	1.283	1.297	1.772	1.797	1.252	0.04	0.01
	S_0	1.377	1.359	1.310	1.804	1.809	1.220	0.06	0.04
CASSCF(10,10)	S_1	1.446	1.283	1.327	1.776	1.791	1.225	0.04	0.03
	S_0	1.385	1.351	1.331	1.800	1.804	1.210	0.04	0.03
				Keto-s-*twist*(−1)					
CASSCF(6,6)	S_1								
	S_0	1.480	1.280	1.272	1.772	1.791	1.236	85.13	82.16
CASSCF(8,8)	S_1	1.469	1.358	1.268	1.773	1.808	1.227	100.94	73.54
	S_0	1.482	1.281	1.263	1.769	1.776	1.240	86.20	82.55
CASSCF(10,10)	S_1	1.484	1.286	1.263	1.756	1.775	1.310	85.28	82.01
	S_0	1.482	1.283	1.263	1.765	1.776	1.244	86.07	82.59
				Keto-s-*trans*(−1)					
CASSCF(6,6)	S_1	1.435	1.287	1.304	1.757	1.773	1.225	179.99	179.99
	S_0	1.367	1.360	1.318	1.788	1.798	1.208	179.96	179.97
CASSCF(8,8)	S_1	1.446	1.298	1.305	1.766	1.773	1.248	179.98	179.96
	S_0	1.369	1.357	1.329	1.792	1.799	1.220	179.92	179.96
CASSCF(10,10)	S_1	1.446	1.274	1.316	1.762	1.771	1.224	179.99	179.92
	S_0	1.371	1.353	1.317	1.788	1.798	1.209	179.83	179.94

state of the three keto forms of $OxyLH_2(-1)$ at the CASSCF-(6,6), (8,8) and (10,10) levels also are presented in Table 1 and Figure 1.

In the lowest-lying singlet excited state, both keto-s-*trans*-(−1) and keto-s-*cis*(−1) have nearly planar ring structures at the CASSCF(6,6), CASSCF(8,8), and CASSCF(10,10) levels. The C2−C2′ bond distance of keto-s-*trans*(−1) and keto-s-*cis*-(−1) are predicted to be 1.446 Å with both the CASSCF(8,8) and (10,10) methods.

Comparing the optimized geometrical parameters of the first singlet excited state (S_1) to the corresponding ground state (S_0), the variations in geometries between these two states are very regular. With three different CAS spaces, the C2−C2′ bond distance in the S_1 state is longer than in the S_0 state. The C−N and C−S bonds in the S_1 state are shorter than in the S_0 state for both planar keto-s-*trans*(−1) and keto-s-*cis*(−1).

For the optimized geometry of the lowest-lying singlet excited-state of keto-s-*twist*(−1), the C2−C2′ bond distance is 1.469 Å with CASSCF(8,8) and 1.484 Å with CASSCF-(10,10). The NCCN and SCCS torsion angles are predicted to be 100.94° and 73.54° with CASSCF(8,8), and 85.28° and 82.01° with CASSCF(10,10). It would be useful to compare these results with those from CASSCF(6,6). Geometry optimizations of the S_1 state at the CASSCF(6,6) level failed. For keto-s-*twist*(−1) optimized at CASSCF(8,8), the variations in geometries from the S_0 state to the S_1 state differ from those of the planar keto forms of $OxyLH_2(-1)$. The C2−C2′ bond length decreases, while the C−N and C−S distances increase. The lowest-lying singlet excited-state of the keto forms of $OxyLH_2$ involves mainly an excitation from HOMO to LUMO.

3.2. Fluorescence Emission Energies of the Anionic Keto Forms of Oxyluciferin. To obtain more accurate energies for the emitting state of the molecules, the MS-CASPT2 method was used to add dynamic electron correlation at the minimized ground and excited state CASSCF geometries. The ground state and lowest-lying singlet excited-state are weighted equally in the state averaging. The same active spaces are used as in the CASSCF geometry optimizations. The ground-state energy is obtained at its first singlet excited-state equilibrium geometry after electronic relaxation to the ground state. The calculated CASSCF and CASPT2 electronic energies of the excited and ground states, CASSCF and CASPT2 vertical emission energies, and CASPT2 emission wavelengths and oscillator strengths with different CAS spaces are given in Table 2.

TABLE 2: Total CASSCF and CASPT2 Electronic Energies, *E* (au), of Anionic Keto Forms of $OxyLH_2(-1)$ for the Ground (S_0) and Lowest-Lying Singlet Excited (S_1) States with Different CAS Spaces, the CASSCF and CASPT2 Vertical Emission Energies, ΔE (kcal/mol), CASPT2 Emission Wavelengths, λ (nm), and Oscillator Strengths *f*

theoretical level	state	E_{CASSCF}	E_{CASPT2}	ΔE_{CASSCF}	ΔE_{CASPT2}	λ	*f*
			Keto-s-*cis*(−1)				
CASSCF(6,6)	S_1	−1435.2098433	−1437.3708363	56.5	58.4	489.5	0.74799
	S_0	−1435.2998294	−1437.4639269				
CASSCF(8,8)	S_1	−1435.2400454	−1437.3706537	55.9	55.6	514.2	0.78780
	S_0	−1435.3291038	−1437.4592644				
CASSCF(10,10)	S_1	−1435.2597140	−1437.3701004	58.4	55.1	519.1	0.89208
	S_0	−1435.3527466	−1437.4578794				
Experiment						545[38−40]	
			Keto-s-*twist*(−1)				
CASSCF(8,8)	S_1	−1435.1820087	−1437.3243325	80.7	68.4	418.3	
	S_0	−1435.3105719	−1437.4332569				
CASSCF(10,10)	S_1	−1435.2033968	−1437.2962948	80.8	79.4	360.2	
	S_0	−1435.3321101	−1437.4228066				
			Keto-s-*trans*(−1)				
CASSCF(6,6)	S_1	−1435.2226705	−1437.3817231	55.3	58.0	492.6	0.65688
	S_0	−1435.3107863	−1437.4742210				
CASSCF(8,8)	S_1	−1435.2586065	−1437.3829946	50.7	54.6	524.0	0.86446
	S_0	−1435.3393218	−1437.4699480				
CASSCF(10,10)	S_1	−1435.2611847	−1437.3833461	57.0	54.2	527.6	0.98434
	S_0	−1435.3520011	−1437.4697052				

Comparing the CASSCF and CASPT2 vertical emission energies, dynamic electron correlation plays an important role in obtaining accurate vertical excited states energies and fluorescent emission energies.

In both the ground and the lowest-lying singlet excited states, keto-s-*trans*(−1) has lower energy than keto-s-*cis*(−1). keto-s-*twist*(−1) has the highest energy and is the transition state for internal rotation between the keto-s-*cis*(−1) and keto-s-*trans*(−1) conformers. CASPT2/CASSCF(8,8) predicts that in the S_0 state, keto-s-*trans*(−1) is 6.7 kcal/mol lower in energy than keto-s-*cis*(−1) and 23.0 kcal/mol lower in energy than keto-s-*twist*(−1). In the S_1 state, keto-s-*trans*(−1) is 7.7 kcal/mol lower in energy than keto-s-*cis*(−1) and 36.8 kcal/mol lower in energy than keto-s-*twist*(−1). CASPT2/CASSCF(10,10) predicts that in the S_0 state, keto-s-*trans*(−1) is 7.4 kcal/mol lower in energy than keto-s-*cis*(−1) and 29.4 kcal/mol lower in energy than keto-s-*twist*(−1). In the S_1 state, keto-s-*trans*-(−1) is 8.3 kcal/mol more stable than keto-s-*cis*(−1) and 54.6 kcal/mol more stable than keto-s-*twist*(−1) at this CASPT2 level. For the S_1 state of the keto-s-*cis*(−1) form, the barriers to internal rotation about the C2−C2′ bond are predicted to be 29.1 and 46.3 kcal/mol at CASPT2/CASSCF(8,8) and CASPT2/CASSCF(10,10). For the S_0 state of keto-s-*trans*(−1), the barriers to internal rotation about the C2−C2′ bond were predicted to be 16.8 kcal/mol with the HF/6-31G* and 19.9 kcal/mol with the B3LYP/6-31+G* methods,[20] which are lower than 23.0 and 29.4 kcal/mol with CASPT2/CASSCF method in the present work. These predictions clearly demonstrate that the keto forms of $OxyLH_2$ in the lowest-lying singlet excited-state have planar rather than twisted structures. The twisted structure is a saddle point on the potential energy surface, which is in contrast to earlier reported AM1 results by McCapra et al.,[4a] who proposed that the twisted keto-anion $OxyLH_2$ was the light emitter.

The vertical emission energies of keto-s-*cis*(−1) are predicted to be 58.4, 55.6, and 55.1 kcal/mol at the CASPT2/CASSCF-(6,6), CASPT2/CASSCF(8,8), and CASPT2/CASSCF(10,10) levels. For keto-s-*trans*(−1), the vertical emission energies are 58.0, 54.6 and 54.2 kcal/mol with the CASPT2/CASSCF(6,6), CASPT2/CASSCF(8,8) and CASPT2/CASSCF(10,10) models. The vertical emission energies of keto-s-*cis*(−1) are very close to those of keto-s-*trans*(−1) at the same theoretical level. The vertical emission energies decrease as the active space increases from (6,6) to (8,8) to (10,10). However, the vertical emission energies for keto-s-*trans*(−1) and keto-s-*cis*(−1) are very close at the CASPT2/CASSCF(8,8) and CASPT2/CASSCF(10,10) levels, which implies that the CAS(8,8) is large enough to describe the spectra of these keto forms of the oxyluciferin system. The predicted vertical emission wavelengths of keto-s-*cis*(-) of 514.2 nm at CASPT2/CASSCF(8,8) and 519.1 nm at CASPT2/CASSCF(10,10) are in good agreement with the experimental value of 545 nm.[38−40] Thus, the emissions of the keto forms of $OxyLH_2(-1)$ are predicted to be green or green-yellow.

It is noteworthy that the vertical emission energies for keto-s-*twist*(−1) are 68.4 and 79.4 kcal/mol at the levels of CASPT2/CAS(8,8) and CASPT2/CAS(10,10) respectively. After carefully checking the electronic configurations of the excited-state of keto-s-*twist*(−1), the CASPT2 results from CAS(8,8) calculations appear more reliable than those based on the CAS(10,10). The geometry optimization for the excited sate of keto-s-*twist*(−1) failed to converge at the CASSCF(6,6) computational level.

The oscillator strengths are in the range of 0.74−0.89 for keto-s-*cis*(−1) and 0.65−0.98 for keto-s-*trans*(−1). Strong $S_1 \rightarrow S_0$ vertical emissions are predicted from the lowest-lying singlet excited-state to the ground state.

To ensure that the correct excited states for keto-s-*cis*-(−1), keto-s-*trans*(−1), and keto-s-*twist*(−1) were located, and that keto-s-*trans*(−1) and keto-s-*cis*(−1) are minima while keto-s-*twist*(−1) is a transition state on the S_1 potential energy surface, vibrational frequency analysis is required at the optimized excited-state geometries. However, in the current version of the MOLCAS program, it is not possible to do such a frequency analysis for state-averaged CASSCF. In order to examine the natures of the S_1 states for the three keto forms of $OxyLH_2(-1)$, CASPT2 single-point calculations on keto-s-*twist*(−1) were performed to determine the lowest-lying excited-state energy at the S_1 state CASSCF(8,8) minimized geometry. During these calculations, the geometrical parameters were fixed except for the SCCS dihedral angle. The energy profile of the first singlet exited state of keto form of $OxLH_2(-1)$ as a function of the SCCS dihedral angle is shown in Figure 2. Figure 2 indicates that the keto-s-*twist*(−1) with a SCCS dihedral angle

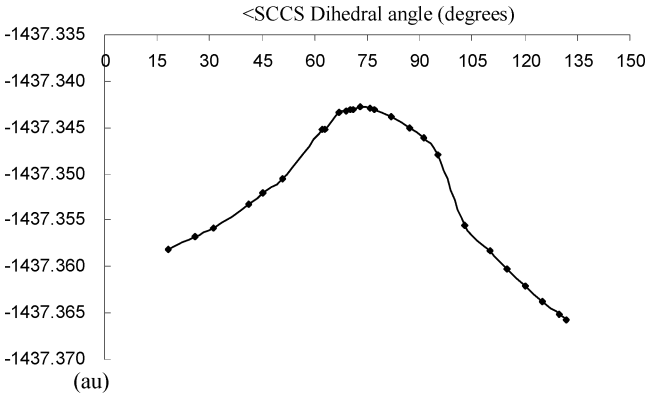

Figure 2. Energy of the lowest-lying singlet excited-state of the keto form of oxyluciferin as a function of the dihedral angle between the rings measured about the C2−C2′ bond at the CASPT2(8,8) level.

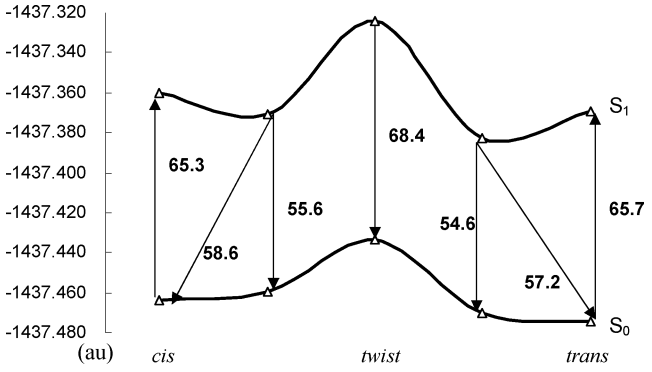

Figure 3. Energy profile for the vertical adsorption, vertical emission and adiabatic emission energies (kcal/mol) for the keto forms of $OxyLH_2(-1)$ at the CASPT2/CASSCF(8,8) level.

of 73° is at the maximum of the potential energy curve, which suggests that the CASSCF(8,8) optimized keto-s-*twist*(−1) is a transition state in the S_1 state.

When the molecule absorbs radiation at its ground state equilibrium geometry to form the excited state, vertical absorption occurs. Table 3 lists the total CASPT2 energies of the S_0 and S_1 states at the optimized S_0 equilibrium geometries and at the optimized S_1 equilibrium geometries at the CASPT2/CASSCF(8,8) theoretical level. The vertical absorption energies, the adiabatic emission energies, and the adsorption wavelengths are present in Table 3.

For keto-s-*cis*(−1), the vertical adsorption energies are predicted to be 70.0, 65.3 and 62.7 kcal/mol, and the adiabatic emission energies 61.2, 58.6, and 59.1 kcal/mol with CAS spaces of (6,6), (8,8), and (10,10) respectively. For keto-s-*trans*(−1), the vertical adsorption energies are 68.6, 65.7 and 62.1 kcal/mol, and the adiabatic emission energies 62.2, 57.2, and 58.4 kcal/mol with CAS spaces of (6,6), (8,8), and (10,10) respectively. The predicted adsorption wavelengths are 408.4 nm at CASPT2/CASSCF(6,6) and 437.8 nm at CASPT2/CASSCF(8,8) for keto-s-*cis*(−1). The comparable predictions are 416.9 nm at CASPT2/CASSCF(6,6) and 435.3 nm at CASPT2/CASSCF(8,8) for keto-s-*trans*(−1). The predictions agree well with the experimental value of 415 nm in water solution at pH=10.[9b] Figure 3 presents the energy profile for vertical adsorption, vertical emission and adiabatic emission of the keto form of oxyluciferin(−1) at CASPT2/CASSCF(8,8).

3.3. Ground and Lowest-Lying Singlet Excited State Geometries of the Anionic Enol Forms of Oxyluciferin. The geometry optimization of the ground and lowest-lying excited states of three possible anionic enol forms of $OxyLH_2$, enol-s-*trans*(−1), enol-s-*cis*(−1), and enol-s-*twist*(−1) were carried out using the same methods as those for the keto forms of $OxyLH_2$-(−1). Selected geometrical parameters of the ground and lowest-lying singlet excited states of the anionic enol forms of oxyluciferin predicted using CASSCF with different active spaces are present in Figure 4 and collected in Table 4. The results indicate that the rings in the enol-s-*trans*(−1) and enol-s-*cis*(−1) are very nearly coplanar at CASSCF(6,6), (8,8), and (10,10) levels. The values of the NCCN and SCCS dihedral angles quantify the very nearly planar structures. Vibrational frequency analysis for the ground state geometries demonstrates that both enol-s-*trans*(−1) and enol-s-*cis*(−1) planar structures are minima since all vibrational frequencies are real. Enol-s-*twist*(−1) is the transition state for internal rotation between enol-s-*cis*(−1) and enol-s-*trans*(−1) with one imaginary frequency. In the S_0 state, CASSCF(6,6), (8,8), and (10,10) predict C2−C2′ bond distances of 1.455, 1.458, and 1.461 Å for enol-s-*cis*(−1), and 1.448, 1.449, and 1.452 Å for enol-s-*trans*(−1). Larger CAS spaces predict slightly longer C2−C2′ bond distances. In the S_1 state, CASSCF(6,6), (8,8), and (10,10) predict C2−C2′ bond distances of 1.440, 1.434, and 1.408 Å for enol-s-*cis*(−1), and 1.426, 1.425, and 1.413 Å for enol-s-*trans*(−1). In the excited state, the larger CAS spaces predict slightly shorter C2−C2′ distances. In contrast to the keto forms,

TABLE 3: Total CASPT2 Electronic Energies at the Optimized S_0 State Equilibrium Geometries, E_{CASPT2_S0} (au), Total CASPT2 Electronic Energies at the Optimized S_1 State Equilibrium Geometries, E_{CASPT2_S1} (au), Vertical Absorption Energies, Adiabatic Emission Energies, ΔE (kcal/mol), and Adsorption Wavelengths, λ (nm), of the Anionic Keto Forms of $OxyLH_2(-1)$ with Different CAS Spaces

theoretical level	state	$E_{CASPT2\_S_0}$	$E_{CASPT2\_S_1}$	ΔE vertical absorption	ΔE adiabatic emission	λ
			Keto-s-*cis*(−1)			
CAS(6,6)	S_1	−1437.3567462	−1437.3708363	70.0	61.2	408.4
	S_0	−1437.4683142	−1437.4639269			
CAS(8,8)	S_1	−1437.3600075	−1437.3706537	65.3	58.6	437.8
	S_0	−1437.4640708	−1437.4592644			
CAS(10,10)	S_1	−1437.3644268	−1437.3701004	62.7	59.1	456.1
	S_0	−1437.4643358	−1437.4578794			
experiment						415[10]
			Keto-s-*trans*(−1)			
CAS(6,6)	S_1	−1437.3715712	−1437.3817231	68.6	62.2	416.9
	S_0	−1437.4808681	−1437.4742210			
CAS(8,8)	S_1	−1437.3694198	−1437.3829946	65.7	57.2	435.3
	S_0	−1437.4741000	−1437.4699480			
CAS(10,10)	S_1	−1437.3774596	−1437.3833461	62.1	58.4	460.5
	S_0	−1437.4763978	−1437.4697052			
experiment						415[10]

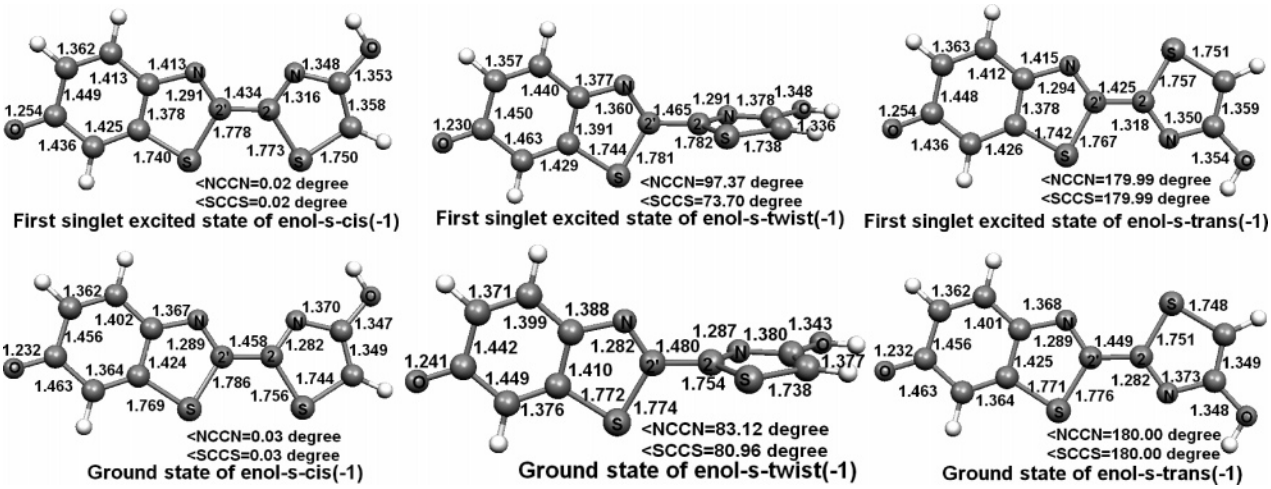

Figure 4. Geometries optimized at the CASSCF(8,8) level for the ground and lowest-lying singlet excited states of anionic enol forms of oxyluciferins.

TABLE 4: Key Geometrical Parameters of the Enol Forms of $OxyLH_2(-1)$ in the Ground (S_0) and Lowest-Lying Singlet Excited (S_1) States Predicted by Different Levels of CASSCF

theoretical level	state	C2−C2′ (Å)	C2′−N (Å)	C2−N (Å)	C2′−S (Å)	C2-S (Å)	C═O (Å)	NCCN (deg)	SCCS (deg)
				Enol-s-*cis*(−1)					
CASSCF(6,6)	S_1	1.440	1.303	1.333	1.806	1.756	1.222	0.06	0.01
	S_0	1.455	1.291	1.290	1.782	1.745	1.227	0.06	0.06
CASSCF(8,8)	S_1	1.434	1.291	1.316	1.778	1.773	1.254	0.02	0.02
	S_0	1.458	1.289	1.282	1.786	1.756	1.232	0.03	0.03
CASSCF(10,10)	S_1	1.408	1.343	1.315	1.793	1.773	1.224	0.12	0.07
	S_0	1.461	1.294	1.281	1.766	1.755	1.236	0.06	0.06
				Enol-s-*twist*(−1)					
CASSCF(6,6)	S_1	1.470	1.366	1.276	1.781	1.775	1.236	98.09	72.32
	S_0	1.480	1.282	1.273	1.771	1.751	1.238	84.28	80.70
CASSCF(8,8)	S_1	1.465	1.360	1.291	1.781	1.782	1.230	97.37	73.70
	S_0	1.480	1.282	1.287	1.774	1.754	1.241	83.12	80.96
CASSCF(10,10)	S_1	1.464	1.360	1.292	1.782	1.788	1.229	98.16	74.82
	S_0	1.479	1.282	1.288	1.774	1.759	1.241	83.10	80.93
				Enol-s-*trans*(−1)					
CASSCF(6,6)	S_1	1.426	1.292	1.325	1.767	1.745	1.254	179.99	180.00
	S_0	1.448	1.290	1.289	1.776	1.740	1.232	179.99	180.00
CASSCF(8,8)	S_1	1.425	1.294	1.318	1.767	1.757	1.254	179.99	179.99
	S_0	1.449	1.289	1.282	1.776	1.751	1.232	180.00	180.00
CASSCF(10,10)	S_1	1.413	1.323	1.336	1.782	1.769	1.222	179.97	179.97
	S_0	1.452	1.289	1.293	1.771	1.756	1.238	180.00	180.00

the lowest-lying excited states of enol-s-*cis*(−1) and enol-s-*trans*(−1) have shorter C2−C2′ bond distances than the ground states. The C−N and C−S bond distances are longer than in the ground states. The −N═C−C═N− fragment with an essentially single C2−C2′ bond becomes more delocalized in S_1 than in S_0.

For the enol-s-*twist*(−1) structure, in the ground state, the C2−C2′ bond distance is 1.480 Å with CASSCF(6,6) or CASSCF(8,8), and 1.479 Å with CASSCF(10,10). In the lowest-lying excited state, the C2−C2′ bond distances are 1.470, 1.465, and 1.464 Å at the CASSCF(6,6), (8,8), and (10,10) levels. A smaller CAS space gives a shorter C2−C2′ bond distance. In the ground state, the NCCN and SCCS torsion angles are 84.28° and 80.70°, 83.12° and 80.96°, and 83.10° and 80.93° with the CASSCF(6,6), (8,8), and (10,10). In the lowest-lying excited state, the NCCN and SCCS torsion angles are 98.09° and 72.32°, 97.37° and 73.70°, and 98.16° and 74.82° with the CASSCF-(6,6), (8,8) and (10,10). Comparing the S_1 and S_0 structures, the C2−C2′ bond distance in the S_1 state is shorter than that in S_0, while the C−N and C−S bond distances are longer than in the ground state. The SCCS dihedral angles of the lowest-lying excited-state are 8.38°, 7.26°, and 6.11° smaller than those in the ground state at the CASSCF(6,6), (8,8), and (10,10) levels. Three CASSCF geometry optimizations with different CAS spaces predict very similar enol-s-*twist*(−1) structures.

The lowest-lying excited states of anionic enol forms of $OxyLH_2(-1)$ involve principally an excitation from the HOMO to the LUMO.

3.4. Fluorescence Emission Spectra of the Anionic Enol Forms of Oxyluciferin. The predicted CASSCF and CASPT2 electronic energies of the lowest-lying singlet excited-state and the ground state, CASSCF and CASPT2 vertical emission energies, and CASPT2 emission wavelengths and oscillator strengths of three anionic enol forms of $OxyLH_2$ with different CAS spaces are collected in Table 5. The ground state energy is obtained after electronic relaxation of the molecule at its first singlet excited-state equilibrium geometry to the ground state.

In both S_0 and S_1, the enol-s-*trans*(−1) has lower energy than enol-s-*cis*(−1). Keto-s-*twist*(−1) is the transition state structure between enol-s-*cis*(−1) and enol-s-*trans*(−1). In the S_0 state, enol-s-*trans*(−1) is 7.1 and 28.3, 5.8 and 26.8, and 2.1 and 19.8 kcal/mol lower than enol-s-*cis*(−1) and enol-s-*twist*(−1) with the CASSCF(6,6), (8,8), and (10,10) methods. In the S_1 state, enol-s-*trans*(−1) is 8.9 and 33.8, 6.5 and 36.1, and 7.2 and 34.0 kcal/mol lower than enol-s-*cis*(−1) and enol-s-*twist*(−1) forms at CASSCF(6,6), (8,8), and (10,10). The barriers to internal

TABLE 5: Total CASSCF and CASPT2 Electronic Energies, *E* (au), of Anionic Enol Forms of $OxyLH_2$ for the Ground (S_0) and Lowest-lying Singlet Excited (S_1) States with Different CAS Spaces, the CASSCF and CSPT2 Vertical Emission Energies, ΔE (kcal/mol), CASPT2 Emission Wavelengths, λ (nm), and Oscillator Strengths *f*

theoretical level	state	CASSCF	CASPT2	ΔE_{CASSCF}	ΔE_{CASPT2}	λ	*f*
			Enol-s-*cis*(−1)				
CASSCF(6,6)	S_1	−1435.1772391	−1437.3445849	63.4	63.2	452.4	
	S_0	−1435.2782942	−1437.4453039				
CASSCF(8,8)	S_1	−1435.2037825	−1437.3476530	58.3	62.1	460.6	0.87680
	S_0	−1435.2966974	−1437.4465843				
CASSCF(10,10)	S_1	−1435.2081638	−1437.3439047	72.1	60.8	470.5	0.86534
	S_0	−1435.3230961	−1437.4407471				
			Enol-s-*twist*(−1)				
CASSCF(6,6)	S_1	−1435.1166289	−1437.3065678	86.6	67.1	426.2	
	S_0	−1435.2546491	−1437.4134794				
CASSCF(8,8)	S_1	−1435.1547408	−1437.3004774	83.7	70.7	404.4	
	S_0	−1435.2881829	−1437.4131338				
CASSCF(10,10)	S_1	−1435.1809440	−1437.3012499	83.7	69.9	409.0	
	S_0	−1435.3142937	−1437.4126513				
			Enol-s-*trans*(−1)				
CASSCF(6,6)	S_1	−1435.1947257	−1437.3587413	56.3	61.4	465.8	0.82436
	S_0	−1435.2843851	−1437.4565570				
CASSCF(8,8)	S_1	−1435.2148940	−1437.3579321	57.1	61.4	465.5	0.82953
	S_0	−1435.3058119	−1437.4558085				
CASSCF(10,10)	S_1	−1435.2380082	−1437.3553660	66.2	55.7	513.2	0.95417
	S_0	−1435.3435805	−1437.4441405				

rotation about the C2−C2′ bond are 33.8, 36.1, and 34.0 kcal/mol for enol-s-*trans*(−1) and 23.9, 29.6, and 26.8 kcal/mol for enol-s-*cis*(−1) predicted with CASPT2/CASSCF(6,6), CASPT2/CASSCF(8,8), and CASPT2/CASSCF(10,10). These predictions indicate that the anionic enol forms of $OxyLH_2$ in the lowest-lying singlet excited-state are planar rather than twisted. The twisted structure is a saddle point on the S_1 potential energy surface.

The vertical emission energies for enol-s-*cis*(−1) are predicted to be 63.2, 62.1, and 60.8 kcal/mol with CASPT2/CASSCF-(6,6), CASPT2/CASSCF(8,8), and CASPT2/CASSCF(10,10). For enol-s-*trans*(−1), the vertical emission energies are 61.4, 61.4, and 55.7 kcal/mol at CASPT2/CASSCF(6,6), CASPT2/CASSCF(8,8), and CASPT2/CASSCF(10,10). The vertical emission energies for enol-s-*twist*(−1) are 67.1, 70.7, and 69.9 kcal/mol at the CASPT2/CASSCF(6,6), CASPT2/CASSCF(8,8), and CASPT2/CASSCF(10,10) levels. The anionic enol forms of $OxyLH_2$ emissions have 15−58 nm longer wavelengths than the anionic keto forms of $OxyLH_2$. The enol forms of the $OxyLH_2(-1)$ have oscillator strengths of 0.82−0.95, which indicate strong $S_1 \rightarrow S_0$ emissions.

To examine the nature of the S_1 states located for the three anionic enol forms of $OxyLH_2$, CASPT2 single-point calculations on enol-s-*twist*(−1) were performed to determine the lowest-lying singlet excited-state energies starting from the CASSCF(8,8) optimized geometry. Calculations were performed using the CAS(8,8) space. The geometry was fixed except for the SCCS dihedral angle. The energy profile for the S_1 state of the enol form of oxyluciferin as a function of the SCCS dihedral angle is shown in Figure 5. The enol-s-*twist*(−1) structure with an SCCS dihedral angle of 74° is at the maxmium of the potential energy curve, which suggests that the CASSCF(8,8)-minimized enol-s-*twist*(−1) structure is a transition state on the S_1 excited state.

Table 6 lists the total CASPT2 energies of the S_0 and S_1 states at the optimized S_0 equilibrium geometries and at the optimized S_1 equilibrium geometries, the vertical adsorption energies, the adiabatic emission energies, and vertical adsorption wavelengths of the anionic enol forms of $OxyLH_2$ at CASPT2/CASSCF with different active spaces. For enol-s-*cis*(−1), the vertical absorption energies are predicted to be 69.4, 67.7, and 64.6 kcal/mol, and the adiabatic emission energies 67.1, 62.5, and 61.2 kcal/mol with active spaces of (6,6), (8,8), and (10,10). For enol-s-*trans*(−1), the vertical absorption energies are 67.2, 67.3, and 60.7 kcal/mol, and the adiabatic emission energies are 61.9, 61.8, and 57.4 kcal/mol with spaces of (6,6), (8,8), and (10,10), respectively. No direct experimental data exists to compare with the predictions. The vertical absorption wavelengths of the anionic enol-structures of $OxyLH_2$ are very close to those of anionic keto-structures of $OxyLH_2$.

Figure 6 presents the energies for vertical adsorption, vertical emission and adiabatic emission of the anionic enol forms of $OxyLH_2$ predicted with the CAS space of (8,8).

The enol-s-*trans*(−1) forms are 15.7 and 11.1 kcal/mol higher in energy than the keto-s-*trans*(−1) structures on the S_1 and S_0 potential energy surfaces. The enol-s-*cis*(−1) species is 14.4 and 10.5 kcal/mol higher in energy than the keto-s-*cis*(−1) structures on the S_1 and S_0 potential energy surfaces.

4. Conclusions

Ab initio CASPT2/CASSCF calculations have been performed on the lowest-lying singlet excited states of two possible light emitters the anionic keto and enol forms of $OxyLH_2$. The geometries of the ground state and the lowest-lying singlet

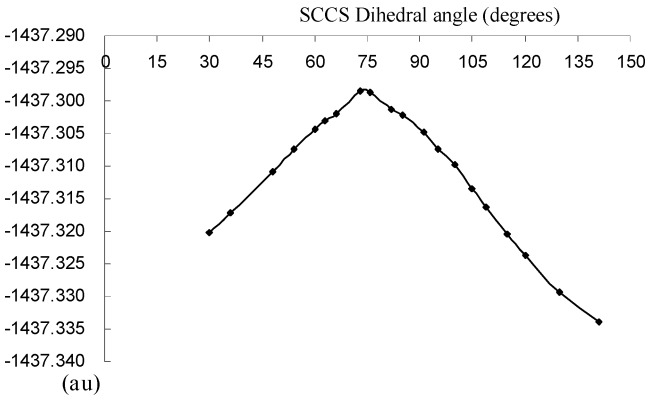

Figure 5. Energy of the lowest-lying singlet excited-state of the enol form of oxyluciferin as a function of the dihedral angle between the rings measured about the C2−C2′ bond at the CASPT2(8,8) level.

TABLE 6: Total CASPT2 Electronic Energies at the Optimized S_0 Equilibrium Geometries, E_{CASPT2_S0} (au), Total CASPT2 Electronic Energies at the Optimized S_1 Equilibrium Geometries, E_{CASPT2_S1} (au), Vertical Absorption Energies, Adiabatic Emission Energies, ΔE (kcal/mol), and Adsorption Wavelengths, λ (nm), of the Anionic Enol Forms of $OxyLH_2$ with Different CAS Spaces

theoretical level	state	$E_{CASPT2\_S_0}$	$E_{CASPT2\_S_1}$	ΔE vertical absorption	ΔE adiabatic emission	λ
			Enol-s-*cis*(−1)			
CAS(6,6)	S_1	−1437.3409323	−1437.3445849	69.4	67.1	411.9
	S_0	−1437.4515365	−1437.4453039			
CAS(8,8)	S_1	−1437.3394354	−1437.3476530	67.7	62.5	422.4
	S_0	−1437.4473125	−1437.4465843			
CAS(10,10)	S_1	−1437.3385398	−1437.3439047	64.6	61.2	442.8
	S_0	−1437.4414492	−1437.4407471			
			Enol-s-*trans*(−1)			
CAS(6,6)	S_1	−1437.3503206	−1437.3587413	67.2	61.9	425.7
	S_0	−1437.4573444	−1437.4565570			
CAS(8,8)	S_1	−1437.3490831	−1437.3579335	67.3	61.8	424.6
	S_0	−1437.4563965	−1437.4558093			
CAS(10,10)	S_1	−1437.3500937	−1437.3553660	60.7	57.4	470.9
	S_0	−1437.4468584	−1437.4441405			

excited-state for the coplanar and the twisted keto and enol forms of anionic $OxyLH_2$ were optimized with the CASSCF method using different sizes of active spaces. Vertical emissions from the relaxed minima of the excited states to the ground states, vertical absorption energies from the ground states geometry, and nonvertical excitation energies have been predicted, together with other characteristics of the transition properties such as oscillator strengths.

The most significant predictions are that the keto and enol forms of anionic $OxyLH_2$ in the lowest-lying singlet excited states have planar structures rather than twisted ones. The twisted structures are saddle point on both the S_0 and S_1 potential energy surfaces. In the S_1 state, the barriers to internal rotation about the C2−C2′ bond are 36.8 kcal/mol for the keto-s-*trans*(−1), 29.1 kcal/mol for keto-s-*cis*(−1), 36.1 kcal/mol for enol-s-*trans*(−1), and 29.6 kcal/mol for enol-s-*cis*(−1) at CASPT2/CASSCF(8,8). A change in color of the light emission upon rotation of the two rings in the S_1 excited-state of $OxyLH_2$ is unlikely as the twisted structure at least for the isolated molecule would relax to the planar minima. In the gas phase, the present prediction rules against the involvement of the twisted keto or enol forms of anionic $OxyLH_2$ in the bioluminescence. Such twisted structures are of high importance in the previously proposed twisted intramolecular charge transfer (TICT) model of oxyluciferin emission. However, the twisted structures are not viable for the isolated molecules according to our present results.

The lowest-lying singlet excited state, S_1, is predicted to lie vertically 54.2−58.4 kcal/mol above the ground state for the anionic planar keto forms of $OxyLH_2$, and 55.7−63.2 kcal/mol above the ground state for the anionic planar enol forms of $OxyLH_2(-1)$. For the anionic twist keto forms of $OxyLH_2$, the S_1 state lies vertically 68.4 kcal/mol above the ground state, while for the anionic twist enol forms of $OxyLH_2$, the S_1 state lie vertically 70.7 kcal/mol above the ground state. Recall, however that the twist structures are not minima in the excited state.

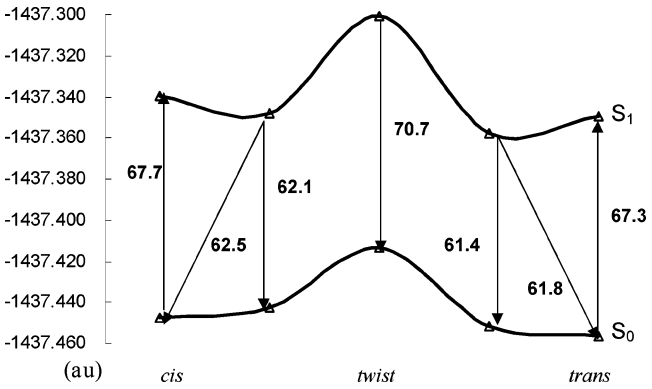

Figure 6. Energy profile for the vertical adsorption, vertical emission and adiabatic emission energies (kcal/mol) for the enol forms of $OxyLH_2(-1)$ at the CASPT2/CASSCF(8,8) level.

The CASSCF and CASPT2 methods have accurately predicted the ground and the lowest-lying singlet excited states geometries, fluorescence emission energies, emission spectra and absorption spectra of anionic oxyluciferins. Our current investigations are based on the gas-phase calculations. Experimental studies have proposed that the emission spectra of oxyluciferines depend on the solvent and the pH conditions. We are investigating the impact of the solvent media around the light emitter on the emission spectra. In addition, the effects of a model of the enzyme active site on the emission spectra are under consideration.

Acknowledgment. Financial support of this research by the Natural Sciences and Engineering Research Council of Canada (NSERC) is gratefully acknowledged. SHARCNET is acknowledged for computing resources.

Supporting Information Available: Cartesian coordinates of all the reported structures are provided as Supporting Information. This material is available free of charge via the Internet at http://pubs.acs.org.

References and Notes

(1) DeLuca, M. *Biochemistry* **1969**, *8*, 160.

(2) White, E. H.; Rapaport, E.; Hopkins, T. A.; Seliger, H. H. *J. Am. Chem. Soc.* **1969**, *91*, 2178.

(3) (a) Branchini, B. R.; Urtiashaw, M. H.; Magyar, R. A.; Portier, N. C.; Ruggiero, M. C.; Stroh, J. G. *J. Am. Chem. Soc.* **2002**, *124*, 2112. (b) Branchini, B. R.; Southworth, T. L.; Murtiashaw, M. H.; Magyar, R. A.; Gonzalez, S. A.; Ruggiero, M. C.; Stroh, J. G. *Biochemistry* **2004**, *43*, 7255.

(4) (a) McCapra, F.; Gilfoyle, D. J.; Young, D. W.; Church, N. J.; Spencer P. In *Bioluminescence and Chemiluminescence: Fundamental and Applied Aspects*; Campbell, A. K., Kricka, L. J., Stanley, P. E., Eds.; Wiley J. & Sons: Chichester, U.K., 1994; p 387. (b) McCapra, F. Mechanisms in Chemiluminescence and Bioluminescence—Unfinished Business. In *Bioluminescence and Chemiluminescence*: *Molucular Reporting with Photons*; Hastings, J. W., Kricka, L. J., Stanley, P. E., Eds.; Wiley J. & Sons: Chichester, U.K., 1996; p 7. (c) McCapra, F. *Methods Enzymol.* **2000**, *305*, 3.

(5) Hastings, J. W. *Gene* **1996**, *173*, 5.

(6) Viviani, V. R. *Cell. Mol. Life Sci.* **2002**, *59*, 1833.

(7) White, E. H.; Rapaport, E.; Seliger, H. H.; Hopkins, T. A. *Bioorg. Chem.* **1971**, *1*, 92.
(8) Branchini, B. R.; Magyar, R. A.; Murtiashaw, M. H.; Anderson, S. M.; Helgerson, L. C.; Zimmer, M. *Biochem.* **1999**, *38*, 13223.
(9) (a) Ugarova, N. N.; Brovko, L. Y. *Russ. Chem. Bull.* **2001**, *50*, 1752. (b) Ugarova, N. N.; Brovko, L. Y. *Luminescence* **2002**, *17*, 321.
(10) Vlasova, T. N.; Leontieva, O. V.; Ugarova, N. N. *Biochemistry (Moscow)* **2006**, *71*, 555.
(11) Gandelman, O. A.; Brovko, L. Y.; Ugarova, N. N.; Chikishev, A. Y.; Shkurimov, A. P. *J. Photochem. Photobiol., B: Biol.* **1993**, *19*, 187.
(12) Brovko, L. Y.; Dementieva, E. I.; Ugarova, N. N. In *Proceedings of the 9th International Symposium*; Hastings, J. W., Kricka, L. J., Stanley, P.E., Eds.; Wiley J. & Sons: Chichester, U.K., 1996; p 206.
(13) Rhodes, W. D.; McElroy, W. D. *J. Biol. Chem.* **1958**, *233*, 1528.
(14) Morton, R. A.; Hopkins, T. A.; Seliger, H. H. *Biochemistry* **1969**, *8*, 1598.
(15) Nakatsu, T.; Ichiyama, S.; Hiratake, J.; Saldanha, A.; Kobashi, N.; Sakata, K.; Kato, H. *Nature* **2006**, *440*, 372.
(16) Jung, J.; Chin, C. A.; Song, P. S. *J. Am. Chem. Soc*. **1976**, *98*, 3949.
(17) Parusel, A. B. J.; Rettig, W.; Sudholt, W. *J. Phys. Chem. A* **2002**, *106*, 804.
(18) Rappoport, D.; Furche, F. *J. Am. Chem. Soc.* **2004**, *126*, 1277.
(19) Foresman, J. B.; Head-Gordon, M.; Pople, J. A.; Frisch, M. J. *J. Phys. Chem.* **1992**, *96*, 135.
(20) Orlova, G.; Goddard, J. D.; Brovko, L. Y. *J. Am. Chem. Soc*. **2003**, *125*, 6962.
(21) Ren, A. M.; Goddard, J. D. *J. Photochem. Photobiol., B* **2005**, *81*, 163.
(22) Gross, E. U. K.; Dobson, J. F.; Petersilka, M. In *Density Functional Theory II*; Nalewajski, R. F., Ed.; Springer: Heidelberg, Germany, 1996; p 81.
(23) Casida, M. E. *Recent Advances in Density Functional Methods*; World Scientific: Singapore, 1995; Part I.
(24) Ren, A. M.; Goddard, J. D. Unpublished results, 2004.
(25) Tozer, D. J.; Amos, R. D.; Handy, N. C.; Roos, B. O.; Serrano-Andres, L. *Mol. Phys.* **1999**, *97*, 859.
(26) Casida, M. E.; Gutierrez, F.; Guan, J.; Gadea, F. X.; Salahub, D. R.; Daudey, J. P. *J. Chem. Phys.* **2000**, *113*, 7062.
(27) Dreuw, A.; Weisman, J. L.; Head-Gordon, M. *J. Chem. Phys.* **2003**, *119*, 2043.
(28) Perdew, J. P.; Zunger, A. *Phys. Rev. B* **1981**, *23*, 5048.
(29) Roos, B. O. *Advances in Chemical Physics: Ab Initio Methods in Quantum Chemistry II*; Lawley, K. P., Ed.; Wiley J. & Sons: New York, 1987; Chapter 69, p 399.
(30) Andersson, K.; Malmqvist, P.-Å.; Roos, B. O.; Sadlej, A. J.; Wolinski, K. *J. Phys. Chem.* **1990**, *94*, 5483.
(31) Andersson, K.; Malmqvist, P.- Å.; Roos, B. O. *J. Chem. Phys.* **1992**, *92*, 1218.
(32) Hariharan, P. C.; Pople, J. A. *Theor. Chim. Acta* **1973**, *28*, 213.
(33) Francl, M. M.; Petro, W. J.; Hehre, W. J.; Binkley, J. S.; Gordon, M. S.; DeFrees, D. J.; Pople, J. A. *J. Chem. Phys.* **1982**, *77*, 3654.
(34) Bernhardsson, A.; Lindh, R.; Olsen, J.; Fulscher, M. *Mol. Phys.* **1999**, *96*, 617.
(35) Malmqvist, P.-Å. *Int. J. Quantum Chem.* **1986**, *30*, 479.
(36) Malmqvist, P.-Å.; Roos, B. O. *Chem. Phys. Lett.* **1989**, *155*, 189.
(37) Karlström, G.; Lindh, R.; Malmqvist, P.-Å.; Roos, B. O.; Ryde, U.; Veryazov, V.; Widmark, P.-O.; Cossi, M.; Schimmelpfennig, B.; Neogrady, P.; Seijo, L. *Comput. Mater. Sci.*, **2003**, *28*, 222.
(38) Wood, K. V.; Lam, Y. A.; Seliger, H. H.; McElroy, W. D. *Science* **1989**, *244*, 700.
(39) Ugarova, N. N. *J. Biolumin. Chemilumin.* **1989**, *4*, 406.
(40) Viviani, V. R.; Bechara, E. J. H. *Photochem. Photobiol.* **1995**, *62*, 490.